Polym. Korea, Vol. 50, No. 3, pp. 410-422 (2026)
https://doi.org/10.7317/pk.2026.50.3.410
ISSN 2234-8077(Online)

나노점토와 알루미나 삼수화물이 친환경 컨베이어 벨트 커버 컴파운드용 천연 고무의 기계적, 열적 및 내화성 특성에 미치는 영향

Mohan Soundarajan*,**,† and Kothandaraman Balasubramanian**,†
*R&D Centre, Thejo Engineering Ltd, Ponneri
**Department of Rubber and Plastic Technology, Anna University
(2025년 7월 23일 접수, 2026년 3월 2일 수정, 2026년 3월 4일 채택)

Effect of Nanoclay and Alumina Trihydrate on the Mechanical, Thermal, and Fire Resistance Properties of Natural Rubber for an Eco-friendly Conveyor Belt Cover Compound

Mohan Soundarajan*,,† and Kothandaraman Balasubramanian****,†**
**R&D Centre, Thejo Engineering Ltd, Ponneri, Chennai-600 067, Tamil Nadu, India*
***Department of Rubber and Plastic Technology, Anna University, Chennai, Tamil Nadu, India*
(Received July 23, 2025; Revised March 2, 2026; Accepted March 4, 2026)

Abstract: This study explores the optimization of organomodified montmorillonites (OMMT)—Cloisite 20A (20A), MAX CT 4260 (CT), and Cloisite SE 3000 (SE)—in combination with alumina trihydrate (ATH) for enhancing natural rubber (NR) formulations used in conveyor belt cover applications. The combined effects of OMMT and ATH on the mechanical, thermal, and flame-retardant properties of NR compounds were systematically evaluated. Morphological characteristics were examined using wide angle X-ray diffraction (WAXD) and scanning electron microscopy (SEM). Polymer-filler and filler-filler interactions were assessed *via* rubber process analyzer (RPA), Dynamic mechanical analysis (DMA), and standard mechanical testing. Flame retardancy and thermal stability were analyzed through limiting oxygen index (LOI), UL-94 horizontal flammability tests, and thermogravimetric analysis (TGA). Additionally, thermal degradation kinetics were investigated using iso-conversional models—Kissinger-Akahira-Sunose (KAS), Flynn-Wall-Ozawa (FWO), and Friedman's method. The results reveal a synergistic enhancement in both flame retardancy and thermal stability with the OMMT-ATH hybrid system, demonstrating its potential as a high-performance filler combination for NR-based conveyor belt cover compounds.

Keywords: natural rubber, nanoclay, intumescent flame retardants, activation energy, thermal degradation kinetics.

Introduction

Fire resistance is a critical consideration for developers of conveyor belts used to transport flammable materials from mining areas to processing locations. Mines are often located in remote areas, and fire accidents, if they occur, are difficult to manage. According to Guo *et al*., the most common causes of ignition in mines are friction, mobile equipment, and electricity.[1] The most frequently encountered flammable substances in mines are coal and the conveyor belt itself. The conveyor belt entry is the most common fire location, and the conveyor belt is the most commonly involved equipment in these fires. According to William *et al*., an average of 10.8 fires occurred per year in the U.S. from 1978 to 1992, with many more unreported incidents.[2,3] Billions of dollars in losses have been reported globally due to conveyor belt fires. In this context, non-metallic rubber parts used in coal and underground mines should be fire-resistant and anti-static (FRAS) materials. Rubber-based conveyor belts are popular and widely used in various industries to transport and process materials. The conveyor belt must be wide, tough, and strong enough to handle heavy loads, especially in mining and metal ore processing. A typical conveyor belt consists of three major components: the top cover, fabric or steel cord reinforcements with skim, and the bottom

†To whom correspondence should be addressed.
bkraman@mitindia.edu, ORCID 0000-0001-7489-6864
mohansoundarajan86@gmail.com, ORCID 0009-0005-2616-6476

cover. The top cover should have good mechanical properties and abrasion resistance.

Regarding halogen-based rubbers and flame retardants, the Consumer Product Safety Commission (CPSC) has banned all organo-halogen flame retardants as a class in certain consumer product categories. The CPSC sought advice from the National Academies of Science, Engineering, and Medicine (NASEM) on the best approach to implement a class-based assessment of organo-flame retardants (OFRs). As part of their 2019 report, NASEM identified 161 OFR chemicals and 1,073 analogues (substances structurally similar to known flame retardants) and recommended a class-based approach to assess hazards for 14 classes of OFRs based on chemical and biological similarity, rather than a monolithic approach for a single OFR class.[4] Several reports are available on this topic, including one by Zhang *et al*., who detailed the environmental fate of 94 halogenated and organophosphate flame retardant replacements. One major drawback of these formulations is that they are halogen-based, making them environmentally harmful.[5-8]

Halogen-free flame retardant materials are considered more environmentally friendly and safer for human health compared to their halogenated counterparts. Many fire-resistant rubber compounds require high loads of metal hydrate fillers or halogen-based flame retardants within the polymer matrix to achieve adequate flame resistance. However, these additions can negatively impact the material's flexibility, mechanical properties, and complicate compounding and processing. NR is the most common polymer used to fabricate conveyor belts, exhibits excellent green strength and good mechanical properties due to its strain-induced crystallization characteristics. The presence of allylic hydrogen in NR accelerates its vulcanization rate compared to other rubbers, contributing to its poor flame retardancy, thermal stability, ozone resistance, and aging characteristics. Many research work has been carried out to study the synergy of nanoclay and ATH in NR or different polymers to study the fire resistant and thermal stability characteristics.[9-16] In this investigation, ATH was integrated with OMMT as a halogen-free flame retardant for NR to achieve a balance of mechanical and fire-resistant properties. NR was chosen as the base matrix, incorporating three different types of organically modified layered nanosilicates: 20A, CT, and SE. The nanoclay material was optimized first, followed by ATH in NR. The mechanical properties, fire resistance, and thermal degradation stability of the rubber compound were then studied under industrial laboratory conditions.

Experimental

Materials. RMA 1X (NR) is a superior quality ribbed smoke sheet was purchased from R1 International, India. 20A, CT and SE are OMMT, these nanoclays were modified with different quaternary ammonium salts by BYK additives, Germany. All other rubber ingredients were industrial grade and were used as received.

Preparation of Rubber Compound. To achieve maximum dispersion, nanoclay masterbatch is prepared by mixing pre-masticated NR and nanoclay in 10:3 ratio at 40 RPM for 4 minutes in banbury. To avoid agglomeration mixing temperature should be maintained at 40 °C. To optimize and evaluate the performance of the above mentioned nanoclays, a basic formulation as per Table 1 is mixed with fill factor of 70% in 1.5 L capacity at 60 RPM for 4 minutes, two wing FARREL BRIDGE lab banbury from England. The final stage of mixing is performed in a CARTER BROS. two-roll mill with a roll speed ratio of 1:1.2, a roll speed of 27.5 RPM, and a nip of 1 mm. The compounds mixed as per Table 1 were characterized using rheological, thermal stability and physical characteris-

Table 1. Formulation for Nanoclay & ATH Optimization

Compound ID	Nanoclays			ATH (F)
	20A	CT	SE	
20A1	1	-	-	-
20A3	3	-	-	-
20A5	5	-	-	-
CT1	-	1	-	-
CT3	-	3	-	-
CT5	-	5	-	-
SE1	-	-	1	-
SE3	-	-	3	-
SE5	-	-	5	-
20A3F25	3	-	-	25
20A3F50	3	-	-	50
20A3F75	3	-	-	75
SE3F25	-	3	-	25
SE3F50	-	3	-	50
SE3F75	-	3	-	75
CT3F25	-	-	3	25
CT3F50	-	-	3	50
CT3F75	-	-	3	75

NR - 100 phr; ZnO - 4 phr; Stearic acid-1.5 phr; ATH-50 phr; Sulphur-2 phr; TBBS-1 phr

tics. After mixing, the compounds were compression molded at 150 °C for optimum curing time which was determined by rheometer studies.

Rheology and curing characteristics were studied in MDR 2000 from Alpha technologies, USA. Tensile and tear tested as per ASTM method in Instron 3400 UTM, USA. Montech Professional MDR 3000 is used for RPA strain sweep measurements. Performed under varying strains amplitude ranges from 0.56% to 100%, a frequency of 1Hz and temperature of 60 °C. Diffraction data were collected in X-ray diffractometer, XRD measurements were performed using a Malvern Panalytical diffractometer with Cu-Kα radiation over a 2θ range of 10.100° at a scan rate of 0.5° min^{-1}. Nanoclay dispersion were studied using QUANTA 200F Scanning electron microscope - Indian Institute of technology, Madras. DMA was conducted on a rectangular specimen (20 × 11 × 1 mm) in tension mode, under varying strain ranges from 0.5 to 7.5% at frequency of 1Hz at 25 °C using DMS6100, SII Nano technology. The horizontal burning test was carried out according to the UL-94 test standard and the specimens used were of dimensions 130 × 13 × 3 mm. LOI is the concentration of oxygen in oxygen/nitrogen mixture in which the material will burn. Atmospheric air contains approximately 21% oxygen it is known in literature, that a material with an oxygen index greater than about 26% will be self-extinguishing. Higher the LOI value better will be the flame retardancy. LOI samples are moulded into the dimension of 150 × 10 × 3 mm as per ASTM D2863 standard. LOI and UL 94 flammability assessments guide the selection and formulation of conveyor belt compounds for fire-prone industrial environments such as power plants and mining operations, and the results of these tests provide valuable preliminary insight into a material's inherent flame spread behaviour, helping identify formulations that are less likely to sustain burning once ignited. The TGA data were obtained under nitrogen atmosphere at a heating rate of 10, 15, 20, and 25 °C/min using PerkinElmer's Pyris 1 Thermogravimetric analyser. In each case 5-10 mg sample was examined under nitrogen gas flow rate of 20 mL/min at the temperatures ranging from room temperature to 750 °C.

Results and Discussion

Optimization of Nanoclays Loading in NR Matrix. Optimization of nanoclay loading within the NR system was done based on the physical and rheological characteristics of the rubber compounds. The compositions were analyzed for rheological and mechanical properties to find optimum loading of each nanoclays within the base formulation and the results are given in the Table 2. Large surface area provided by the silicate layers and the organomodifiers on the nanoclay can promote the effective interaction of the nanomaterials with the isoprene macromolecules.[11,15] This can ultimately enhance the mechanical properties of the compound prepared using organically modified layered silicates and polymers.[11,15-18] In addition to that, organomodifiers also has an impact on the sulphur vulcanization of rubbers as they can act as promoters for crosslinking process. Quaternary ammonium salts used for layered silicate modification involves in reaction rate determining step of ZnO-amine transition state formation during vulcanization and accelerates the rate of curing.[15,19-21]

Considering rheological analysis of the rubber compounds prepared in comparison with the base formulation, MH values were found to increase with increase in nanoclay loading irrespective of the type of the organo modifier in the clay. 20A has a nonpolar alkyl ammonium part of dimethyl dihydrogenated tallow ammonium cations with a packing of 95 meq/100 g nanoclay. The organic tallow can interact with the NR soft segments to ensure better interaction in the compound. This can promote the crosslinking process and corresponding viscosity. While, CT and SE have layered magnesium aluminum phyllosilicate structure, which also can promote the interaction between the filler and matrix. Relative to the base formulation, 1 phr nanoclay caused a reduced ts2 and T90 values considerably, irrespective of nature of the modifier of the nanoclay particles. This indicates the decrease in scorch safety and improved cure rate of the composite. Also, the increase in cure rate has a linear relationship with the loading of nanoclay initially and reached optimum with 3 phr filler content. 1 phr nanoclay loading tends to increase the hardness by 11-13 units with respect to the base formulation. Reinforcing effect of nanoclay is reflected in hardness and mechanical properties. The enhanced tensile strength, further points towards the improved reinforcement with the matrix. This will ultimately enhance the effective stress transfer in between the matrix and filler. Based on the rheological and physical properties obtained, a nanoclay loading of 3 phr was selected as optimal. The corresponding compounds incorporating this 3 phr nanoclay were then used for further detailed characterizations.

Optimization of ATH in NR-nanoclay Compound. The three optimized compositions of 20A, CT, and SE nanoclays (as shown in Table 1) were further mixed with ATH at loadings of 25, 50, and 75 phr in order to achieve compositions

Table 2. Rheological and Mechanical Properties of NR Compounds in Comparison with the Base Formulation

Parameters	RC[a]	20A1	20A3	20A5	CT1	CT3	CT5	SE1	SE3	SE5
Rheology @ 150 °C										
MH (dNm)	7.38	8.28	8.31	8.72	8.49	8.59	8.52	8.03	7.76	7.66
ts2 (min)	6.43	1.84	1.41	1.40	1.88	1.39	1.39	2.17	1.78	1.57
T90 (min)	12.74	4.83	4.52	4.67	4.94	4.83	4.79	5.08	4.92	4.72
Hardness (Shore A)	39	52	56	59	53	57	60	49	51	54
Tensile strength (MPa)	22.8	24.2	25.5	25.1	24.8	26.4	23.7	23.2	24.6	23.5
Elongation (%)	701	614	642	631	613	637	580	615	654	677
Tear strength (kgf/cm)	36.6	47.1	51.1	47.5	43.1	42.2	45.9	41.3	41.8	45.6

[a]RC contains no ATH filler

Table 3. Rheological Properties and Mechanical Properties of Rubber Compounds with Nanoclay and ATH (3 phr nanoclay + 25, 50 and 75 phr of ATH Loading Respectively)

Characteristics	20A3F25	20A3F50	20A3F75	CT3F25	CT3F50	CT3F75	SE3F25	SE3F50	SE3F75
Rheology @ 150 °C									
MH (dNm)	9.88	12.20	13.65	10.10	12.48	15.00	9.17	10.91	12.93
ts2 (min)	1.02	0.89	0.85	1.39	1.22	1.05	1.08	1.01	0.91
T90 (min)	4.09	4.36	3.86	4.82	4.73	4.73	4.64	4.00	3.89
Hardness (Shore A)	58	61	63	60	64	69	54	59	63
Tensile strength (MPa)	24.5	23.2	17.7	23.9	21.4	16.0	24.1	25.1	17.9
Elongation (%)	669.9	597.5	591.1	651.5	580.6	558.3	650.1	617.7	601.0
Tear strength (kgf/cm)	39.2	39.5	36.6	40.4	40.6	38.2	36.1	38.1	37.2

which are more similar to the actual conveyor belt compounds. The samples were tested for rheological and physical properties which are tabulated in Table 3 to identify the optimum formulation which then could be tested for thermal stability. From the results in Table 3 with increase in ATH loading from 25, 50, and 75 parts, ts2 and T90 of the rubber compounds increased gradually. Rubber compound with 20A and CT nanoclays along with ATH, showed higher MH and hardness than SE nanoclay containing compounds in every respective ATH loading.

20A and CT nanoclays loaded compounds observed as comparably stiffer and brittle than SE nanoclay loaded compound. Hydrophilic ATH and hydrophobic matrix could have minimal interaction during the composite formation which reflected in MH and physical properties. As a result, tensile and tear strength decreases gradually with respect to ATH loading. Low strain modulus values were found similar for all the rubber compounds. Tear resistance didn't show any significant effect with ATH loading from 25 and 50 phr. However, further increases in ATH loading beyond 50 phr result in a reduction in tear strength due to the dilution of rubber by ATH. With increasing ATH loading, the dilution effect diminishes the rubber volume fraction—and thus reduces crosslink density per unit volume—leading to a lower effective crosslink density and a subsequent decline in mechanical properties.

On the other hand, a loading of 50 phr ATH offers a favorable balance, enhancing flame-retardant properties without significantly compromising mechanical performance. This level of ATH has been demonstrated to enhance the composite's overall physical performance, rendering it well-suited for conveyor belt applications and their related standards, where both flame resistance and mechanical strength are essential.

Rubber Processing Analysis. In RPA, the response of rubber compound to the strain amplitude by storage modulus (G'), generally found to be nonlinear. At constant temperature, the modulus of rubber compounds decreases significantly with increasing strain amplitude due to the breakdown of weak filler–filler networks at lower strain amplitudes of 0.1-20%, which can be explained by the Payne effect.[16,17] In the current study, within 20-100% strain the storage modulus (G') drop gradually for all the formulations. The drop of storage modulus

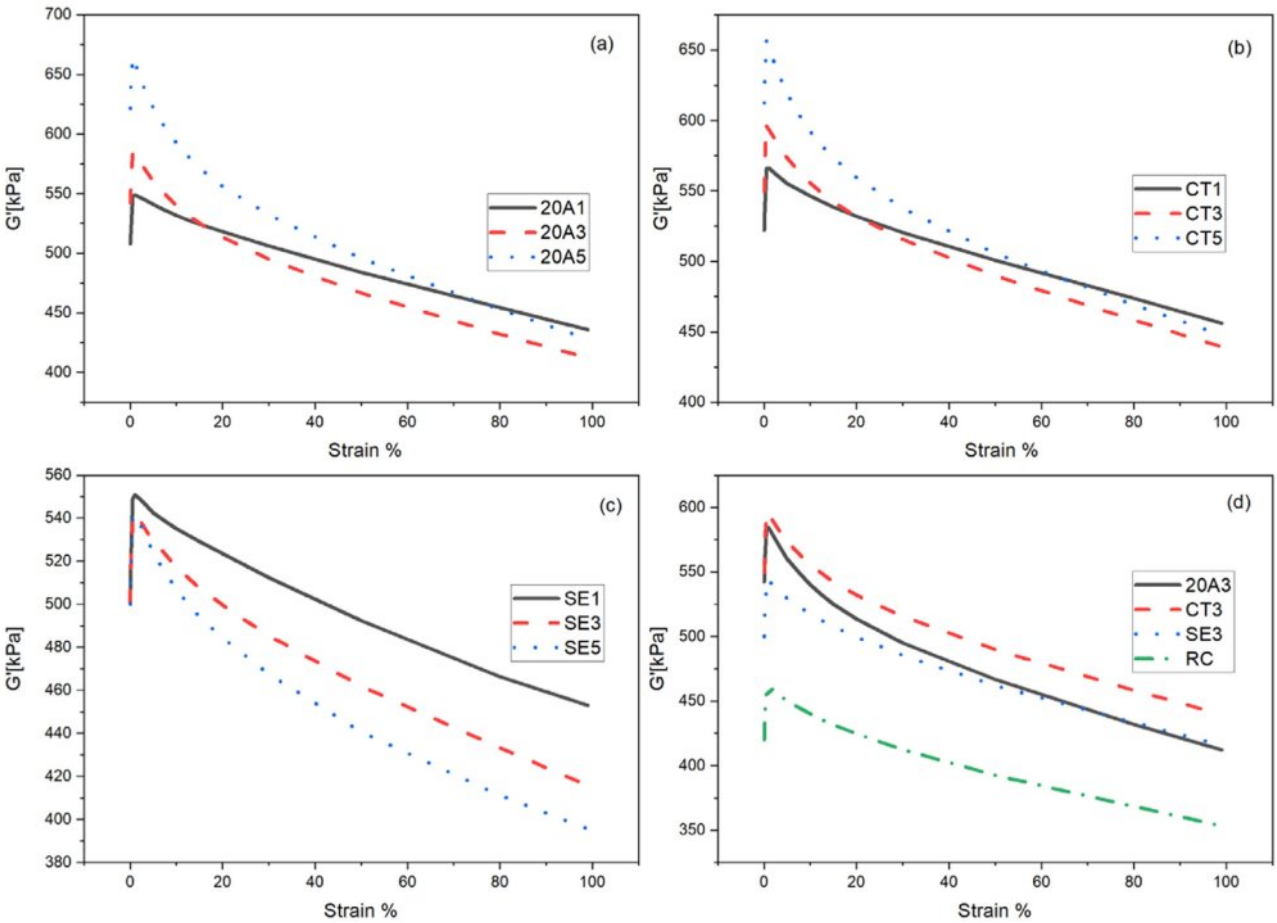

Figure 1. Graph of RPA storage modulus (G') as a function of strain amplitude for rubber compounds with different nanoclay loading (1, 3, and 5 phr): (a) 20A; (b) CT; (c) SE; (d) 3 phr of nanoclay in NR compared with Neat-NR (RC).

from 0.1-20% of strain is also gradual due to the effective filler-filler interaction and polymer chain entanglement, which is displayed in Figure 1(a-c). However, increased loading of nano fillers often leads to a higher probability of slippage filler-filler and filler-matrix interphases due to the agglomeration. Irrespective of the type of nanoclay, compounds with 3 phr loading show minimal loss in storage modulus. Comparing the three nanoclays with the neat NR compound (Figure 1(d)), the SE3 compound showed the closest to neat NR, suggesting the most effective reduction in filler-filler networking. Lower decrements in shear modulus (G') typically indicates better dispersion of fillers in the polymer matrix which can also reflects in improved compound processability and reduced energy consumption during mixing. Overall, RPA studies showed that nanoclay interacted better with the polymer in SE than in CT, and CT was better than 20A.

X-ray Diffraction Studies. To evaluate the nanoclay dispersion, WAXD is performed, and the results demonstrated optimum properties. Rubber compounds prepared using three different nanoclays at 3 phr loading were subjected to morphological analysis. Table 4 indicates a significant improvement in basal spacing compared to the raw nanoclays, suggesting effective exfoliation and/or intercalation of the silicate layers within the

Table 4. WAXD Results of Nanoclay Incorporated NR Compounds

Sample ID	Description	2θ (°)	D spacing (Å)
20A	Pristine Nanoclay	19.941	4.453
CT	Pristine Nanoclay	16.314	5.433
SE	Pristine Nanoclay	20.167	4.403
20A3	3 phr in NR	18.610	4.764
CT3	3 phr in NR	12.949	6.831
SE3	3 phr in NR	12.920	6.848
20A3F50	3 phr in NR+50 phr ATH	18.332	4.836
CT3F50	3 phr in NR+50 phr ATH	18.205	4.869
SE3F50	3 phr in NR+50 phr ATH	19.110	4.640

NR matrix.[22-26] The percentage of interstitial expansion reflects the degree of separation of the silicate layers within the polymer matrix. For example, a 40% interstitial expansion for 20A indicates that the nanoclay layers in the compound have expanded by 40% relative to their initial spacing.

Similarly, SE and CT exhibit approximately 60% expansion within their respective compounds.[27] A decrease in 2θ values corresponds to an increase in the spacing between the crystal planes of the nanoclay, which is indicative of exfoliation or intercalation. After adding 50 parts of ATH to the 20A3F50 nanoclay compound, the d-spacing values of 20A nanoclay decreased marginally, and the levels of intercalation and exfoliation remained largely unchanged. However, in the case of SE3F50 and CT3F50, the d-spacing decreased by 25%, which can be attributed to the hindrance caused by the ATH particles. These particles interfere with the interaction between the rubber polymer chains and the magnesium aluminum phyllosilicate nanoclays (CT and SE), resulting in less efficient exfoliation. The ATH particles may act as physical barriers, obstructing the intercalation of the rubber matrix between the clay layers, which leads to a reduction in the 2θ values compared to the nanoclay composite in NR compound.

SEM Analysis. The dispersion of the nanoclay fillers was further analyzed through micrograph imaging. The uniform distribution of the reinforcing fillers 20A, CT, and SE was confirmed using SEM, as shown in Figures 2(a-d). Tensile fracture specimens were examined to evaluate the dispersion pattern, which also provides insights into the fracture mechanisms of the rubber compounds synthesized in this study. In the SEM image, the exfoliated clay layers look like lines in the rubber compound and are marked with white circles, while the ZnO/Zinc stearate particles are shown with yellow circles.The incorporation of 20A and CT nanoclays into NR leads to a reduction in elasticity, resulting in lower elongation at break, as reflected in the mechanical performance data. This decreased flexibility increases brittleness, as evidenced by the smoother fracture surfaces observed in the tensile fracture SEM images (Figure 2(a) and 2(b)) of the 20A3 and CT3 compounds. In contrast, the surface modifier present in SE nanoclay forms strong intermolecular interactions with the NR matrix in the SE3 compound. This interaction promotes a cavitation-driven failure mechanism accompanied by significant elastic deformation prior to fracture, as seen in the tensile fracture SEM image (Figure 2(c)).[28-31] A similar fracture morphology is observed for the neat NR compound (Figure 2(d)), indicating elastic behaviour. This behaviour suggests that SE nanoclay reinforcement more effectively enhances the mechanical performance of the SE3 compound. Furthermore, the tensile fracture morphology indicates that SE nanoclay exhibits better dispersion within the NR matrix compared to 20A and CT nanoclays.

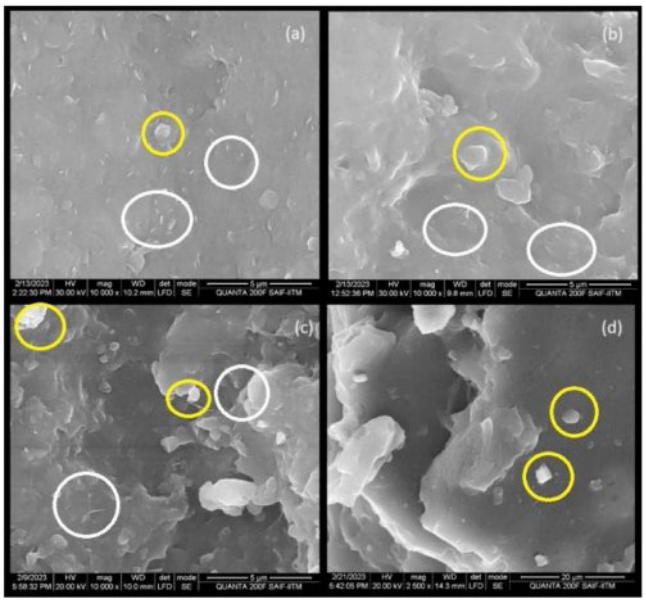

Figure 2. Scanning electron microscopy tensile fracture of the composites: (a) 20A; (b) CT; (c) SE; (d) Base (RC) – without nanoclays.

Dynamic Mechanical Analysis. To understand the effect of various fillers used to modify the flammability characteristics on the viscoelastic performance of the formulation, DMA was employed on the optimized formulations. Since rubber is a viscoelastic material, its elastic properties are measured by the storage modulus (E'), and its viscous properties by the loss modulus (E''). The ratio of E'' to E' gives the loss factor, tan δ. DMA was conducted in tension mode at a frequency of 1 Hz. The storage modulus (E'), loss modulus (E''), and tan δ were obtained through a strain sweep ranging from 0.5% to 7.5% at 25 °C, and the responses are shown in Figure 5(a-c).

Compared to the base formulation, the inclusion of nanoclays enhanced both E'' and tan δ, indicating improved energy dissipation and damping characteristics. In particular, the storage modulus (E') exhibited a pronounced decrease with increasing strain, as shown in Figure 3(a) phenomenon known as the Payne effect. This behavior is attributed to the progressive breakdown of weak physical networks formed by filler-filler interactions, especially in the case of nanoclay-based fillers.[22,23,30,31] Among the nanoclays evaluated, 20A and CT exhibited higher stiffness at low strain levels, suggesting stronger initial filler-filler interactions relative to the SE nanoclay. As strain increased, the breakdown of these networks resulted in a significant reduction

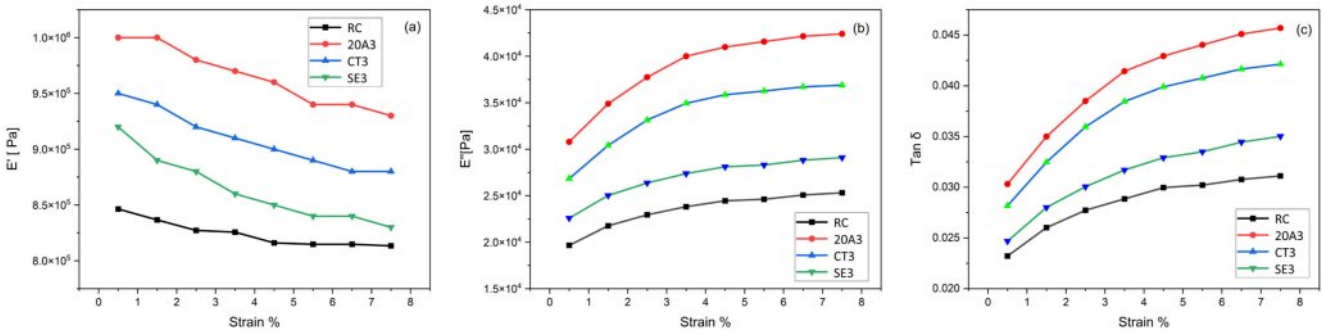

Figure 3. DMA of rubber compounds at difference strain amplitude of 20A, CT & SE: (a) Storage modulus; (E'); (b) loss modulus (E''); (c) tan δ.

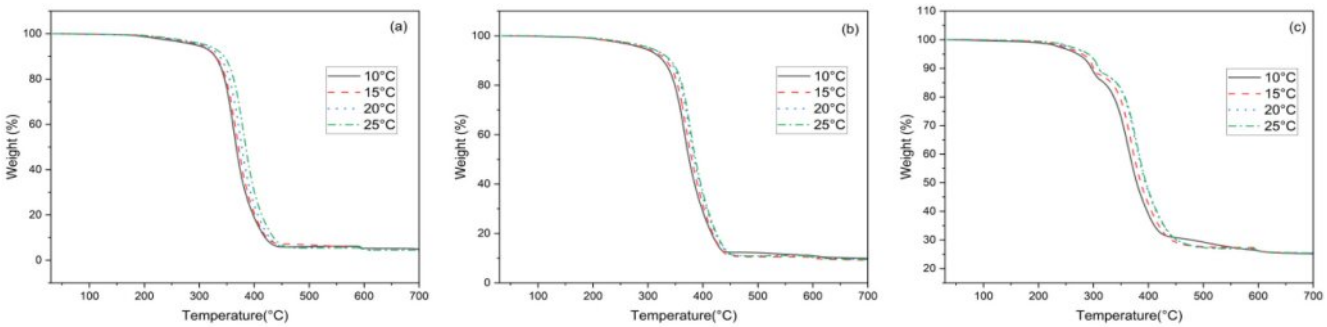

Figure 4. TGA plot of (a) RC; (b) SE3; (c) SE3F50 at heating rate of 10, 15, 20, and 25 °C/min.

in storage modulus. The extent of this decrease is indicative of the filler dispersion: a greater drop corresponds to more agglomerated filler structures.

The SE nanoclay, modified with specific surface treatments, exhibited enhanced interaction with the polymer matrix. This led to lower E'' and tan δ values across all strain amplitudes, reflecting reduced hysteresis and consequently lower heat buildup under cyclic loading. Such behavior is particularly advantageous for dynamic applications, such as conveyor belts, where maintaining structural integrity under cyclic or heavy loads is critical. The trends observed in DMA measurements were consistent with those obtained from RPA results. Furthermore, tensile failure morphology provided additional evidence for the disruption of the filler network, validated its significant influence on the viscoelastic properties of the compound.

UL94 Flammability and LOI. The flammability characteristics, including the synergistic effects of three different nanoclays (SE, CT, and 20A) at their optimal loadings in combination with ATH, were evaluated using the UL94 horizontal flammability test and the LOI method. For comparison, both a base NR compound and a halogen-free NR formulation were tested under the same condition.

All specimens were tested at a standardized thickness of 3 mm in accordance with the UL94 protocol. Under the test conditions, all samples exhibited complete combustion. To ensure consistency, each specimen was ignited for 30 seconds, and the burning rate was calculated by recording the time required to combust a 75 mm length of the sample. These results are summarized in Table 5.

Table 5. Horizontal Flammability - UL94 and LOI Characteristics of Nanoclay/ATH/NR Composites

Parameters	Horizontal burning test		LOI (%)
	Avg. Burning time (min)	Avg. Burning rate (mm/min)	
RC	1.40	54.01	16.5
20A3F25	2.96	25.49	17.5
20A3F50	3.91	19.86	18.3
20A3F75	5.46	14.71	20.1
CT3F25	3.11	24.46	17.7
CT3F50	4.66	18.02	18.8
CT3F75	5.32	14.59	20.3
SE3F25	3.07	24.27	17.7
SE3F50	4.17	16.22	19.0
SE3F75	5.41	14.45	20.6

Incorporation of 3 phr nanoclay and 25 phr ATH into the base NR formulation led to a noticeable reduction in the burning rate, approximately halving it—demonstrating a significant improvement in flame-retardant performance.[11,14,32] The addition of ATH consistently decreased the self-extinguishing time across all formulations, regardless of the nanoclay type, highlighting the effectiveness of ATH in enhancing fire resistance.

The three nanoclays SE, CT, and 20A exhibited comparable synergistic effects with ATH. This was further supported by LOI results. The oxygen index increased from 16.5 for the unfilled compound to 17.5 with the addition of 25 phr ATH, independent of the nanoclay type. When ATH content was further increased to 75 phr, the LOI increased significantly to 20.6, again showing no substantial variation between different nanoclay types. These findings, as presented in Table 5, confirm the fire-resistant performance of the conveyor belt compound while nanoclays contribute to the flame-retardant effect, the overall enhancement is primarily driven by the ATH content, with the nanoclays acting as co-synergists that further improve the fire performance of the system.

Thermogravimetric Analysis to Study Thermal Degradation Kinetics. TGA was carried out to evaluate the thermal stability of the new formulations. The compounds were subjected to TGA in the temperature range of 30-750 °C at inert atmosphere at different heating rate of 10, 15, 20, and 25 °C to study the thermal degradation kinetics and the respective thermograms in Figure 4. All the samples showed an initial weight loss of adsorbed water molecule removal within a region of 150 °C. Compared to the base formulation, the incorporation of nanoclay and ATH significantly improved the final degradation temperature and demonstrated a synergistic effect, enhancing char-forming characteristics as expected from the flammability analysis. Also, the ash content has been significantly improved with the increase filler level. The delayed thermal degradation of various compound is attributed to the improved thermal resistant characteristics of the final formulations due to the "tortoise" mechanism of thermal conductivity impregnated by each filler within the network system of matrix macromolecules and fillers.[26-29,31,32] Detailed analysis of improved thermal stability in line with the improved flame-retardant characteristics has been evaluated through thermal degradation kinetic study in the following section. Based on the current analysis SE outperformed 20A and CT in terms of morphological analysis and mechanical properties, leading to the SE used rubber compounds being subjected to thermal degradation kinetics. The kinetics of the thermal degradation process of NR, SE3, and SE3F50 composites was studied, SE3F50 compound showed a balanced mechanical and fire resistant property than SE3F25 and SE3F75 compound. Thermal degradation of NR is very complex and several research works has been investigated it for NR[36] and other polymers.[34] Many methods are available to study the thermal degradation kinetics of polymer composites; among them, the KAS, FWO, and Friedman methods are the most recent and consistent approaches.[33-38] A Aboulkes et al studied thermal degradation kinetics of PE and PP using KAS, FWO, Friedmann and other isoconversional methods.[36] TGA is one of the best methods to study the thermal degradation kinetics of polymer composites. In the past decade, number of kinetic studies have been done with different heating rates for determining the rate constants (k), activation energy (E_a), reaction order (n), R is Universal gas constant (J/mol K) and Arrhenius pre-exponential factor (A).

In the present work, the three isoconversional methods—KAS, FWO, and Friedman—were used to estimate the activation energy and to assess the robustness and reproducibility at various conversion rates under different heating rates (10, 15, 20, and 25 °C) for RC, SE3, and SE3F50. The corresponding thermograms are shown in Figure 4(a–c).

The reaction rate can be described in terms of the following equation using rate constant k and reaction model f(α).

$$\frac{d\alpha}{dt} = kf(\alpha) \tag{1}$$

The conversion rate α can be determined by the following equation

$$\alpha = \frac{W_0 - W_t}{W_0 - W_f} \tag{2}$$

Where W_0, W_t and W_f are the weight of the sample at initial degradation, at the time of 't' and final degradation respectively. According to Arrhenius equation, the rate constant 'k' is given by

$$k = A.e^{-(Ea/RT)} \tag{3}$$

Equation (1) becomes

$$\frac{d\alpha}{dt} = A.e^{-(Ea/RT)}f(\alpha) \tag{4}$$

Equation (4) describes the relationship between the reaction rate, conversion rate and at temperature T. The heating rate (°C/min) and change in temperature with respect to time, are used to conduct the kinetic study in TGA as per the equation. Equation (3) can be written as follows:

$$\frac{d\alpha}{dt} = \frac{A}{\beta} \cdot e^{-(Ea/RT)} f(x) \quad (5)$$

Equation (4) and (5) are the most fundamental equations used for kinetic studies of thermal degradation. Isoconversion methods have been mostly used to determine the Ea of polymer by kinetic studies as a function of conversion rate without any previous assumption of the kinetic model. FWO method and KAS method has been used to estimate the activation energy at a given conversion rate with different heating rates.

KAS equation (6):

$$\ln\frac{\beta}{T^2} = \ln\frac{RA}{E_a g(\alpha)} - \frac{E_a}{RT} \quad (6)$$

β – heating rate (°C/min), T – Temperature, E_a – Activation energy, R – Universal gas constant

From the above equation activation energy is calculated by plotting the graph between against for various degree of conversion and different heating rates. Activation energy was calculated from the graph Figure 5(a–c) and listed in the Table 6, along with the corresponding R^2 values for RC, SE3, and SE3F50. Using the KAS method, activation energies were determined for RC, SE3, and SE3F50, yielding values of 178 kJ/mol, 396 kJ/mol, and 158 kJ/mol, respectively. In the case of the SE3, the layered SE nanoclay forms a protective barrier over the polymer, enhancing thermal stability and increasing its activation energy by a factor of two relative to RC. For SE3F50, the ATH in the composite removes water molecules during heating, resulting in a decrease in activation energy at a conversion rate of 0.2. In a typical flame-retardant composite, one would expect a synergistic interaction between nanoclay and ATH to increase

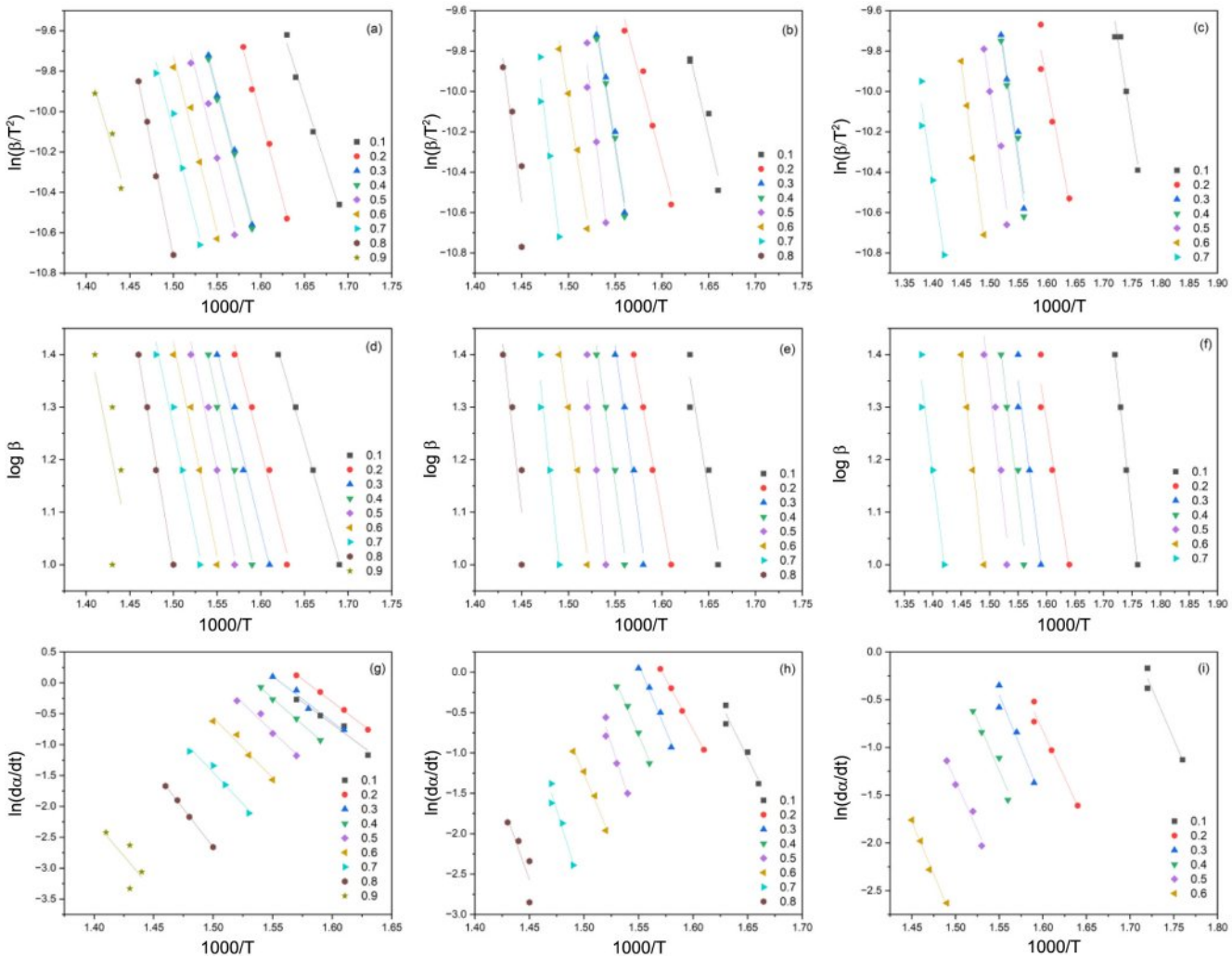

Figure 5. KAS model for conversion rate at 0.1 to 0.9 for (a) RC; (b) SE3; (c) SE3F50; FWO model for conversion rate at 0.1 to 0.9 for (d) RC; (e) SE3; (f) SE3F50 and Friedman's model for conversion rate at 0.1 to 0.9 for (g) RC; (h) SE3; (i) SE3F50

Table 6. Activation Energy (E_a) and R2 Value Obtained from KAS, FWO and Friedmans' Method

Conversion rate			0.1	0.2	0.3	0.4	0.5	0.6	0.7	0.8
KAS Method	RC	E_a	104.9	130.2	128.6	128.9	134.8	145.6	159.2	178.4
		R^2	0.990	0.999	0.994	0.994	0.992	0.990	0.981	0.964
	SE3	E_a	149.3	202.1	245.7	246.3	263.0	284.6	315.3	396.5
		R^2	0.962	0.988	0.988	0.986	0.993	0.995	0.986	0.997
	SE3F50	E_a	173.5	103.2	162.3	162.8	181.0	164.3	158.3	-
		R^2	0.950	0.995	0.970	0.969	0.999	0.988	0.963	-
FWO's Method	RC	E_a	98.9	120.5	127.0	132.7	138.4	148.8	161.9	180.4
		R^2	0.995	0.994	0.996	0.995	0.993	0.992	0.984	0.968
	SE3	E_a	149.3	157.0	245.7	246.3	263.0	284.6	315.3	396.5
		R^2	0.962	0.940	0.988	0.989	0.993	0.995	0.986	0.997
	SE3F50	E_a	180.8	128.1	155.2	165	186.8	175.9	161.8	-
		R^2	0.979	0.964	0.980	0.973	0.998	0.972	0.968	-
Friedman's Method	RC	E_a	100.5	121.1	125.7	131.7	142.6	162.9	185.7	202.3
		R^2	0.995	0.995	0.996	0.992	0.989	0.990	0.978	0.951
	SE3	E_a	208.7	235.5	257.3	269.3	285.4	314.4	354.3	388.8
		R^2	0.992	0.987	0.987	0.995	0.995	0.994	0.967	0.899
	SE3F50	E_a	180.0	163.6	180.3	175.1	171.9	177.1	180.0	-
		R^2	0.970	0.980	0.975	0.968	0.962	0.968	0.970	-

the activation energy of thermal degradation, because the high inorganic content helps in forming a more stable char barrier, which retards degradation. This expectation aligns well with the improvements observed in the UL94 flammability and LOI tests. The endothermic dehydration of ATH absorbs heat and reduces heat transfer within the system, enhancing flame retardancy, but the release of chemically bound water and the associated mass loss can create a pseudo-effect that may appear as a reduced onset of decomposition temperature of the SE3F50 compound (this appears as a shoulder in the TGA trace at around 300 °C in Figure 4(c)).

FWO equation (7):

$$\log\beta = \left[\log\frac{AE_a}{R} - \log f(\alpha) - 2.315\right] - 0.4567\frac{E_a}{RT} \quad (7)$$

β – heating rate (°C/min), T – Temperature, E_a – Activation energy, α – Conversion factor, R – Universal gas constant, A– .pre-exponential factor. FWO method is an integral method and the activation energy of RC, SE3, and SE3F50 are determined from the slope of 0.4567 straight-line plots (Figure 5(d-f)) of log β against for various degrees of conversion. The activation energies and corresponding R^2 values for RC, SE3, and SE3F50, as determined using the FWO method, are presented in Table 6, exhibiting a trend consistent with that observed from the KAS method.

Friedman equation (8):

$$\ln\frac{d\alpha}{dt} = A\ \ln f(\alpha) - \frac{E_a}{RT} \quad (8)$$

β – heating rate (°C/min), T – Temperature,
E_a – Activation energy, α – Conversion factor,
R – Universal gas constant, A – pre-exponential factor

FWO is an integral method by plotting against at various heating rates will get a straight line and E_a is calculated from the slope (Figure 5(g-i)). The peak activation energies for RC, SE3, and SE3F50 demonstrate a trend consistent with the results obtained from both the KAS and FWO methods, as shown in Table 6. The E_a values calculated using the KAS, FWO, and Friedman methods are consistent and in close agreement, as strongly supported by this study, with R^2 values ranging from 0.90 to 1.00. Plotting the conversion rate against activation energy for all three methods yields similar patterns, with the results being nearly identical, as depicted in Figure 6. The activation energy (E_a) of all samples increases considerably with the conversion rate for RC and SE3; however, in the case of SE3F50, it decreases

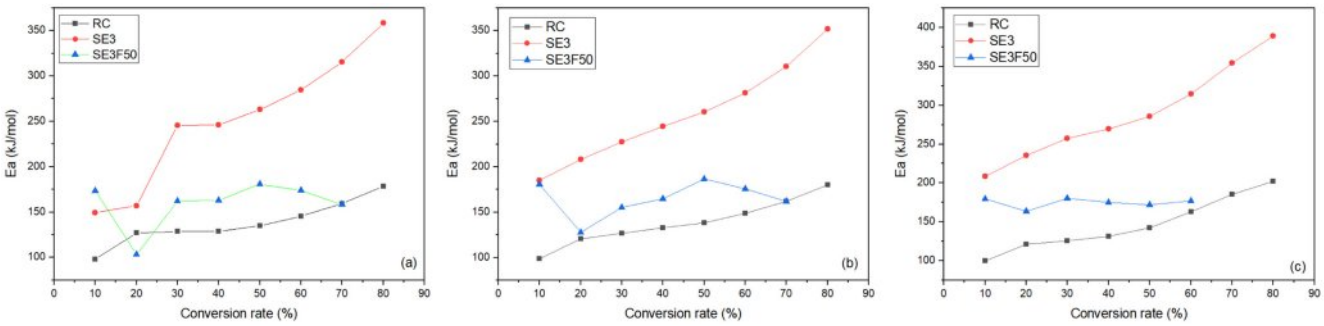

Figure 6. Activation energy (E_a) *vs*. Conversion rate from (a) KAS; (b) FWO; (c) Friedman's method.

at conversion rates of 0.2, 0.6, and 0.7. The dehydration of ATH in the composite causes a significant dip in activation energy at a conversion rate of 0.2, and the spherical nature of alumina is unable to effectively protect the polymer surface, resulting in a slight reduction in thermal stability at conversion rates of 0.6 and 0.7.

Based on isoconversional kinetic analyses (KAS, FWO, Friedman), the apparent E_a of SE3 is roughly twice that of RC, indicating that the SE nanoclay affords substantially better thermal degradation stability. This enhanced degradation stability reduces the likelihood of generating smaller, more flammable fragments during heating or combustion. The inclusion of ATH significantly decreases the thermal degradation stability compared to the nanoclay composite; however, it still outperforms RC. Moreover, incorporation of nanoclay and ATH enhances both the thermal stability and flame-retardant performance of the NR compounds, exceeding the base formulation and approaching the requirements for FRAS conveyor belt cover compounds.

Conclusions

Nanoclays tend to increase the vulcanization rate, mechanical property and thermal degradation stability of the compounds. RPA and DMA studies revealed the interaction of OMMT with NR matrix at low strain amplitude at constant temperature, especially SE nanoclay recorded excellent interaction with NR and ultimately resulted in best reported values for physical properties. Tensile fracture analysis using SEM and X-ray diffraction studies revealed the exfoliated and intercalated rubber compound was formed. The synergy of nanoclay/ATH in NR rubber compound shows an improvement in fire-resistant characteristics results as evidenced by the horizontal burning test in UL94 flammability and limiting oxygen index improved to 20.6%, much higher than base formulation. From the TGA, thermal degradation kinetics has been studied using KAS, FWO and Friedman method, SE nanoclay improved thermal stability of NR significantly with an activation energy of 390 kJ/mol at a 0.8 conversion rate and the estimated activation energies are closely relatable and R2 value is closer to "1". The synergistic effect of SE3F50 compound results in a reduction of activation energy (E_a) by an average of 180 kJ/mol at a 0.8 conversion rate, closely approximating the value observed for the neat NR compound. The endothermic dehydration of ATH enhances flame retardancy by absorbing heat and improving initial thermal resistance, the associated loss of hydrate molecules can adversely affect the thermal degradation stability of the SE3F50 compound. Further optimization of the composite is necessary to improve its fire resistance and thermal degradation stability, aiming for an environmentally friendly fire resistant rubber compound that maintains a balanced mechanical performance suitable for FRAS conveyor belting cover application.

Acknowledgments: We express our sincere gratitude to the Management of Thejo engineering Ltd, Chennai for allowing us to use the facilities for conducting the research work. I would like to express my sincere gratitude to Dr. P. J. Jandas of the Laboratory for Chemistry and Life Sciences, Institute of Innovative Research (IIR), Tokyo Institute of Technology, R-1-17, 4259, Yokohama, 226-8501, Japan, for their invaluable support and expertise throughout the course of this research.

Conflict of Interest: Hereby declares that the authors do not have any sort of conflict/competing of interest about this research article.

References

1. Guo, X.; Liu, X.; Gardoni, P.; Glowacz, A.; Królczyk, G.; Incecik, A.; Li, Z. Machine Vision Based Damage Detection for

Conveyor Belt Safety Using Fusion Knowledge Distillation, *Alex. Eng. J.*, **2023**, 71, 161-172.
2. William, H. Pomroy and Annie M. Carigiet; Analysis of Underground Coal Mine Fire Incidents in the United States from 1978 through 1992. United States Bureau of Mines information circular 1995.
3. Draganová, K.; Semrád, K.; Spodniak, M.; Cúttová, M. Innovative Analysis of the Physical-mechanical Properties of Airport Conveyor Belts. *Transp. Res. Procedia*, **2020**, 51, 20-27.
4. Bevington, C.; Williams, A. J.; Guider, C.; Baker, N. C.; Meyer, B.; Babich, M. A.; Robinson, S.; Jones, A.; Phillips, K. A. Development of a Flame Retardant and an Organohalogen Flame Retardant Chemical Inventory. *Sci. Data* **2022**, 9, 295.
5. Zhang, X.; Sühring, R.; Serodio, D.; Bonnell, M.; Sundin, N.; Diamond, M. L. Novel Flame Retardants: Estimating the Physical-chemical Properties and Environmental Fate of 94 Halogenated and Organophosphate PBDE Replacements. *Chemosphere*, **2016**, 144, 2401-2407.
6. Li, T. Y.; Ge, J. L.; Pei, J.; Bao, L. J.; Wu, C. C.; Zeng, E. Y. Emissions and Occupational Exposure Risk of Halogenated Flame Retardants from Primitive Recycling of E-Waste. *Environ Sci. Technol*. **2019**, 5, 12495-12505.
7. Oh, J.; Shibulal, G. S.; Mensah, B.; Ahn, D. U.; Kim, S. J.; Jeong, K. U.; Nah, C. Lifetime Prediction of Flame Retardant-filled Ethylene-propylene-diene-termonomer Rubber Compounds. *Polym. Korea*, **2015**, 39, 795-800.
8. Nah, C.; Oh, J.; Mensah, B.; Jeong, K.-U.; Ahn, D. U.; Kim, S.-J.; Lee, Y.; Nam, S.-H. Effects of Thermal Aging on Degradation Mechanism of Flame Retardant-filled Ethylene-propylene-diene Termonomer Compounds. *J. Appl. Polym. Sci.* **2014**, 132, 41324.
9. Wan, L.; Deng, C.; Zhao, Z. Y.; Chen, H.; Wang, Y. Z. Flame Retardation of Natural Rubber: Strategy and Recent Progress. *Polymers*. **2020**, 12, 429.
10. Liangqing Lai, Jia Liu, Zhen Lv, Tianming Gao, Yongyue Luo, Recent advances for flame retardant rubber composites: Mini-review, Advanced Industrial and Engineering Polymer Research, Volume 6, Issue 2, 2023, Pages 156-164, ISSN 2542-5048.
11. Cho, B. H.; Hwang, I. R.; Lee, Y. S.; Jeong, J. M.; Son, K. J.; Nah, C. Enhancement of Flame Retardancy of Rubber Matrix Using Nanofillers. *J. Nanosci Nanotechnol*. **2008**, 8, 5516-20.
12. Chang, M.-K.; Hwang, S.-S.; Liu, S.-P. Flame Retardancy and Thermal Stability of Ethylene-vinyl Acetate Copolymer Nanocomposites with Alumina Trihydrate and Montmorillonite. *J. Industrial Eng. Chem.*, **2014**, 20, 1596-1601.
13. Nie, Y.; Qu, L.; Huang, G.; Wang, X.; Weng, G.; Wu, J. Homogenization of Natural Rubber Network Induced by Nanoclay. *J. Appl. Polym. Sci*. **2014**, 131, 40324.
14. Zhang, H.; Wang, Y.; Wu, Y.; Zhang, L.; Yang, J. Study on Flammability of Montmorillonite/StyreneButadiene Rubber (SBR) Nanocomposites. *J. Appl. Polym. Sci.* **2005**, 97, 844-849.
15. Sasikumar, S.; Sivaram, S. K.; Yadav, P. K.; Murugesan, S. Review on the Development of Natural Rubber/nanoclay Nanocomposites, In Micro and Nano Technologies, Nanoclay-Based Sustainable Materials. *Elsevier*, **2024**, 77-89.
16. He, S.; Xue, Y.; Lin, J.; Zhang, L.; Du, X.; Chen, L. Effect of Silane Coupling Agent on the Structure and Mechanical Properties of Nano-dispersed Clay Filled Styrene Butadiene Rubber. *Polym. Compos*, 2014.
17. Jia, Q.-X.; Wu, Y.-P.; Wang, Y.-Q.; Lu, M.; Yang, J.; Zhang, L.-Q. Organic Interfacial Tailoring of Styrene Butadiene Rubber–Clay Nanocomposites Prepared by Latex Compounding Method. *J. Appl. Polym. Sci.* **2007**, 103, 1826-1833.
18. Bandyopadhyay, A.; Thakur, V.; Pradhan, S.; Bhowmick, A. K. Nanoclay Distribution and Its Influence on the Mechanical Properties of Rubber Blends, *J. Appl. Polym. Sci.*, **2010**, 115, 1237-1246.
19. López-Manchado, M. A.; Arroyo, M.; Herrero, B.; Biagiotti, J. Vulcanization Kinetics of Natural Rubber–organoclay Nanocomposites, *J. Appl. Polym. Sci.*, **2003**, 89, 1-15.
20. Javier, C.-G.; Retsos, H.; Verdejo, R.; Toki, S.; Hsiao, B. S.; Giannelis, E. P.; López-Manchado, M. A. Effect of Nanoclay on Natural Rubber Microstructure. *Macromolecules* **2008**, 41, 6763-6772.
21. Azizli, M. J.; Ziaee, M.; Rezaeinia, S.; Seyfi, J.; Mansourian-Tabaei, M.; Hoseinzadeh, M.; Azizli, M. H. Studying the Roles of Nanoclay and Blend Composition on the Improved Properties of Natural Rubber/chloroprene Composites, *Polym. Compos*. **2018**, 39, 1562-1574.
22. Lopattananon, N.; Tanglakwaraskul, S.; Kaesaman, A.; Seadan, M.; Sakai, T. Effect of Nanoclay Addition on Morphology and Elastomeric Properties of Dynamically Vulcanized Natural Rubber/ Polypropylene Nanocomposites. *Int. Polym. Process.* **2014**, 29, 332-341.
23. Rao, V. S.; Yadav, V.; Kumar, V. K.; Chand, N. Combined Effect of Nanoclay and Alumina Addition on Structure, TGA, DMA Characteristics of Nanoclay, and Alumina-filled Polypropylene Nanocomposites. *J. Thermoplastic Compos. Mater*. **2011**, 25, 851-863.
24. Malik, N.; Kumar, P.; Ghosh, S. B.; Shrivastava, S. Organically Modified Nanoclay and Aluminum Hydroxide Incorporated Bionanocomposites towards Enhancement of Physico-mechanical and Thermal Properties of Lignocellulosic Structural Reinforcement. *J. Polym. Environ.* **2018**, 26, 3243-3249.
25. Mohan, T. P.; Kuriakose, J.; Kanny, K. Effect of Nanoclay Reinforcement on Structure, Thermal and Mechanical Properties of Natural Rubber–styrene Butadine Rubber (NR–SBR). *J. Industrial Eng. Chem.*, **2011**, 17, 264-270.
26. Liu, Y.; Li, L.; Wang, Q. Effect of Carbon Black/nanoclay Hybrid Filler on the Dynamic Properties of Natural Rubber Vulcanizates. *J. Appl. Polym. Sci.*, **2010**, 118, 1111-1120.
27. Dharmaraj, M. M.; Chakraborty, B. C.; Begum, S.; Natarajan, R.; Chandramohan, S. Effect of Nanoclay Reinforcing Filler in Nitrile Rubber/polyvinyl Chloride Blend: Frequency Response of Dynamic Viscoelasticity and Vibration Damping. *Iran Polym. J*. **2022**, 31, 1247-1261.
28. Yahaya, L. E.; Adebowale, K. O.; Menon, A. R. R. Mechanical Properties of Organomodified Kaolin/natural Rubber Vulcanizates.

Appl. Clay Sci., **2009**, 46, 283-288.
29. Wang, Y.; Zhang, H.; Wu, Y.; Yang, J.; Zhang, L. Preparation and Properties of Natural Rubber/rectorite Nanocomposites. *Europ. Polym. J.* **2005**, 41, 2776-2783.
30. Sun, Y.; Luo, Y.; Jia, D. Preparation and Properties of Natural Rubber Nanocomposites with Solid-state Organomodified Montmorillonite. *J. Appl. Polym. Sci.*, **2008**, 107, 2786-2792.
31. Doğan, Mehmet & Oral, Demet & Yılmaz, Betül & Savu, Melih & Karahan, Selçuk & Bayramlı, Erdal. Physical Properties and Cure Characteristics of Natural Rubber/Nanoclay Composites with Two Different Compatibilizers. *J. Appl. Polym. Sci*., **2011**, 121, 1530-1535.
32. Younis, A. A.; El-Wakil, A. A. Improvement of Mechanical and Flame Retardant Properties of Natural Rubber by Eco-friendly Watermelon Peel and Crumb Rubber. *Fibers Polym.* **2021**, 22, 1237-1246.
33. Cheng, K.-C.; Yu, C.-B.; Guo, W.; Wang, S.-F.; Chuang, T.-H.; Lin, Y.-H. Thermal Properties and Flammability of Polylactide Nanocomposites with Aluminum Trihydrate and Organoclay. *Carbohyd. Polym.* **2012**, 87, 1119-1123.
34. Redaoui, D.; Sahnoune, F.; Heraiz, M.; Raghdi, A. Mechanism and Kinetic Parameters of the Thermal Decomposition of Gibbsite $Al(OH)_3$ by Thermogravimetric Analysis, 6th International Congress & Exhibition (APMAS2016), Maslak, Istanbul, Turkey, June 1–3, 2016.
35. Sajna, V. P.; Mohanty, S.; Nayak, S. K. A Study on Thermal Degradation Kinetics and Flammability Properties of Poly (lactic acid)/Banana Fiber/Nanoclay Hybrid Bionanocomposites. *Polym. Compos.*, **2017**, 38, 2067-2079.
36. Aboulkas, A.; El harfi, K.; El Bouadili, A. Thermal Degradation Behaviors of Polyethylene and Polypropylene. Part I: Pyrolysis kinetics and mechanisms.
37. He, Canzhong, Wang, Yueqiang, Luo, Yongyue, Kong, Lingxue and Peng, Zheng. Thermal Degradation Kinetics and Mechanism of Epoxidized Natural Rubber. *J. Polym. Eng.*, **2013**, 33, 331-335.
38. Lucie Tibiletti, Claire Longuet, Laurent Ferry, Philippe Coutelen, André Mas, Jean-Jacques Robin, José-Marie Lopez-Cuesta, Thermal Degradation and Fire Behaviour of Unsaturated Polyesters Filled with Metallic Oxides, *Polym. Degradation and Stability* **2011**, 96, 67-75.